THE ASTROPHYSICAL JOURNAL, 387:417–429, 1992 March 1

A SURVEY OF N_2H^+ IN DENSE CLOUDS: IMPLICATIONS FOR INTERSTELLAR NITROGEN AND ION-MOLECULE CHEMISTRY

M. WOMACK,[1] L. M. ZIURYS,[2,3] AND S. WYCKOFF[1]
Received 1991 May 30; accepted 1991 September 4

ABSTRACT

Spectra of the N_2H^+ $J = 1 \rightarrow 0$, $J = 3 \rightarrow 2$ and $^{15}NNH^+$ and $N^{15}NH^+$ $J = 1 \rightarrow 0$ rotational transitions have been obtained toward a sample of star-forming and cold dark clouds in the Galaxy. Toward the star-forming regions, line profiles are relatively narrow (typically 1–5 km s^{-1}) and show no evidence of line wings, in contrast to the spectra of HCO^+. The apparent absence of N_2H^+ in hot, shocked gas suggests that this ion may be a selective tracer of extended, quiescent material. Column densities of N_2H^+ were found to be $N_{tot} \sim 5 \times 10^{12}$ cm^{-2} toward cold clouds and $N_{tot} \sim 10^{14}$ cm^{-2} toward warm clouds. These values correspond to fractional abundances, relative to H_2, of $f \sim 4 \times 10^{-10}$ toward both the warm and cold clouds. Such abundances agree well with predictions of quiescent cloud ion-molecule chemistry models, provided "steady state," not "early time" values are used. Thus, the abundance and distribution of N_2H^+ is well-explained by ion-molecule chemistry, provided it has reached steady state, as is found for interstellar NH_3. In contrast, most abundances of simple interstellar molecules are better reproduced by models calculated for early times. The N_2H^+ results thus are further evidence that interstellar nitrogen chemistry is anomalous.

Subject headings: ISM: abundances — ISM: molecules — molecular processes

1. INTRODUCTION

The interstellar molecular ion, N_2H^+, was first observed by Turner (1974) toward several warm clouds and tentatively identified by Green, Montgomery, & Thaddeus (1974). This identification was made on the basis of calculations of the molecule's quadrupole hyperfine structure in the $J = 1 \rightarrow 0$ rotational transition produced by the spin of the outer nitrogen nucleus. The identification was later confirmed by Thaddeus & Turner (1975), who observed spectra of the $J = 1 \rightarrow 0$ line toward OMC-2, which showed the hyperfine lines due to the spin of the inner nitrogen atom as well. The nitrogen-15 isotopic species, $^{15}NNH^+$ and $N^{15}NH^+$, were first observed by Linke, Guélin, & Langer (1983) who detected their fundamental transitions toward DR 21(OH).

N_2H^+ is predicted by chemical models of dense clouds to be formed primarily by ion-molecule reactions, which proceed quickly at low temperatures because they are generally exothermic and contain negligible activation energies. The major route to the formation of N_2H^+ in dense gas is the reaction:

$$N_2 + H_3^+ \rightarrow N_2H^+ + H_2 , \quad (1)$$

which proceeds at the Langevin rate, $k_1 = 1.8 \times 10^{-9}$ cm^3 s^{-1} (Herbst & Klemperer 1973). In fact, virtually all of the N_2H^+ comes from this reaction (Nejad, Williams, & Charnley 1990). The molecule is thought to be destroyed in regions of very high density [$n(H_2) > 10^6$ cm^{-3}] and high temperature ($T_K >$ 200 K) where the ion undergoes dissociative electron recombination,

$$N_2H^+ + e^- \rightarrow N_2 + H \quad (2)$$

at a rate $k_2 = 1.6 \times 10^{-6}$ cm^3 s^{-1}, recently measured at 110 K (Amano 1990).

Because they can be produced at such low temperatures, molecular ions are thought to be key species in interstellar chemistry. The only molecular ion in dense clouds which is well-studied thus far is HCO^+. In contrast with predictions of ion-molecule chemical models, HCO^+ often appears to have large abundances in hot outflow material such as that associated with Orion, in addition to being present in regions of quiescent material (e.g., Vogel et al. 1984). Curiously, recent observations of N_2H^+ toward Orion show that this ion is found exclusively in the undisturbed ridge gas (Womack, Ziurys, & Wyckoff 1991). These data suggest a differing chemical behavior between two very common interstellar ions that is not predicted by ion-molecule models. Detailed knowledge of the characteristics of N_2H^+ emission in other molecular clouds is thus essential for understanding ion-molecule chemistry.

N_2H^+ is of interest from another aspect. Despite the high cosmic abundance of nitrogen in the galaxy, the chemistry of nitrogen-bearing molecules in interstellar clouds is somewhat anomalous. While most observed molecular abundances in dense gas are reproduced fairly well by ion-molecule models of only $\sim 10^5$ yr, or at so-called "early times" (Brown & Rice 1986), ammonia abundances are better predicted by models of clouds of $\sim 10^6$–10^7 yr, or when steady state is reached (Millar et al. 1988; Herbst & Leung 1989). In order to better elucidate the nature of nitrogen chemistry, abundances of more molecules containing this element need to be determined. N_2H^+ is an important species to study in this regard. Furthermore, since it is formed directly from molecular nitrogen, knowledge of the abundance of N_2H^+ should directly reflect the amount of N_2 present in dense gas, which as yet remains unknown.

A survey of N_2H^+ in molecular clouds had previously been performed by Turner & Thaddeus (1977) using the NRAO 36 foot (11 m) telescope. However, at the time these data were taken, receiver sensitivities were poor by comparison with those of the present. Also, Turner & Thaddeus observed only the $J = 1 \rightarrow 0$ transition of N_2H^+. Consequently, estimates of the abundances and distribution of this ion could be improved upon. Their observations indicated that N_2H^+ emission is generally optically thin with narrow line widths.

[1] Department of Physics and Astronomy, Arizona State University, Tempe, AZ 85287.
[2] Department of Chemistry, Arizona State University, Tempe, AZ 85287.
[3] Presidential Young Investigator.

In order to better determine the chemistry of N_2H^+, and nitrogen-containing molecules in general, we have conducted a renewed survey of N_2H^+ via its $J = 1 \rightarrow 0$ and $J = 3 \rightarrow 2$ transitions, as well as the $J = 1 \rightarrow 0$ transition of its nitrogen-15 isotopes toward various star-forming regions and several dark clouds using the National Radiation Astronomy Observatory (NRAO) 12 m telescope. Here we present our data, including N_2H^+ abundances, and discuss their implications for both ion-molecule and nitrogen chemistry.

2. OBSERVATIONS

Spectra of the $J = 1 \rightarrow 0$ rotational transition of N_2H^+ at 93.17358 GHz, $^{15}NNH^+$ at 90.26383 GHz, and $N^{15}NH^+$ at 91.20600 GHz, and the $J = 3 \rightarrow 2$ transition of N_2H^+ at 279.5117 GHz were obtained with the NRAO 12 m telescope[4] on Kitt Peak in 1990 March. At 93 GHz, the half-power beamwidth (HPBW) of the telescope was 70″ and the beam efficiency, η_c, was 0.88. The receiver consisted of a dual-channel, cooled SIS mixer, which was tuned to reject the image sideband. At 279 GHz, the beamwidth was 25″, $\eta_c = 0.35$, and the receiver was a dual-channel, cooled Schottky diode mixer. In this case, a single-sideband filter was used to reject the image sideband. The IF frequency in all cases was 1.5 GHz and data were taken in the upper sideband. Temperature scales were established by the chopper-wheel method in terms of T_R^*. The line radiation temperatures, T_R, were determined from the corrected antenna temperatures, T_R^*, where $T_R = T_R^*/\eta_c$.

The backends for the 3 mm observations were two 128 channel filterbanks with 250 kHz (0.80 km s^{-1}) resolution and two 128 channel filters with 100 kHz (0.32 km s^{-1}) resolution for the N_2H^+ $J = 1 \rightarrow 0$ data. Two 128 channel filterbanks with 1 MHz (3.3 km s^{-1}) resolution were used for the isotopes, $^{15}NNH^+$ and $N^{15}NH^+$. The 1 mm data were obtained with either two 256 channel 1 MHz (1.07 km s^{-1}) filterbanks or two 256 2MHz (2.15 km s^{-1}) filterbanks. Two filterbanks were necessary for each receiver channel in all cases. The spectra were taken in a position-switching mode, with the reference position 30′ west in azimuth.

Observations of the $J = 1 \rightarrow 0$ transitions of N_2H^+ and the nitrogen-15 isotopes were performed toward all of the sources listed in Table 1. The $J = 3 \rightarrow 2$ transition of N_2H^+ was observed toward the warm clouds only. The coordinates of the clouds observed are given in Table 1.

3. RESULTS

The N_2H^+ $J = 1 \rightarrow 0$ rotational transition at 93.17358 GHz exhibits a quadrupole hyperfine structure due to the spin of the two nitrogen nuclei. The outer nitrogen nucleus produces three hyperfine components, $\Delta F_1 = 0$ (93.171881 GHz), $\Delta F_1 = -1$ (93.173777 GHz), and $\Delta F_1 = +1$ (93.176310 GHz) (Cazzoli et al. 1985). The inner nitrogen nucleus is responsible for further splitting of the $\Delta F_1 = 0$ and $\Delta F_1 = -1$ components into three lines each, less than 250 kHz apart. The frequencies and statistical weights of these hyperfine lines are given in Table 2.

The structure of the $J = 1 \rightarrow 0$ transition of N_2H^+ is shown clearly in the spectra obtained with 100 kHz resolution toward the cold clouds L134 N and TMC-1 (Fig. 1). The local thermodynamic equilibrium (LTE) relative line strengths are shown beneath the spectrum of L134 N. The $J = 1 \rightarrow 0$ transition observed toward the dark clouds ρ Oph and Orion (3N, 1E) is shown in Figure 2. Toward most of the warmer clouds, only the hyperfine structure due to the outer nitrogen nucleus could be resolved in the $J = 1 \rightarrow 0$ transition of N_2H^+. The top panels of Figures 3–14 show this transition observed with 250 kHz resolution toward the following warm sources: Orion-KL, Orion-S, DR 21(OH), W3(OH), NGC 7538 IRS 1, NGC 7538 IRS 11, NGC 7538, W51 N, W51 M, W49, Sgr B2(OH) and Sgr B2 N. The $J = 1 \rightarrow 0$ transition was newly detected toward W49. No anomalous hyperfine ratios were observed in the $J = 1 \rightarrow 0$ transition toward any of the sources. Line temperatures, LSR velocities, and linewidths of the N_2H^+ $J = 1 \rightarrow 0$ spectra are presented in Table 3.

The $J = 3 \rightarrow 2$ transition of N_2H^+ at 279.5117 GHz was detected toward the warm clouds listed above, using 1 MHz resolution, with the exception of Orion-KL, which was observed with 2 MHz resolution. The hyperfine splitting of this transition due to the outer nitrogen nucleus is calculated to be less than ~ 500 kHz and that due to the inner nitrogen nucleus is even smaller (Sastry et al. 1981). Thus the hyperfine structure of the $J = 3 \rightarrow 2$ transition could not be resolved in these spectra. The $J = 3 \rightarrow 2$ spectra are shown in the middle panels of Figures 3–14. Toward L134 N, an upper limit of $T_R < 1.4$ K was achieved for the $J = 3 \rightarrow 2$ line. The $J = 3 \rightarrow 2$ line was newly detected toward all the sources. Measured quantities of the $J = 3 \rightarrow 2$ emission are presented in Table 4.

Spectra were also obtained of the two nitrogen-15 isotopes, using resolutions of 250 kHz and 1000 MHz and are shown in the bottom panels of Figures 3–14. As the figures shown, the $^{15}NNH^+$ $J = 1 \rightarrow 0$ transition (90.263833 GHz) was detected toward the following sources: NGC 7538 IRS 11, NGC 7538

TABLE 1

SOURCE COORDINATES

Source	α(1950.0)	δ(1950.0)
W3(OH)	2^{h}23^{m}17^s.0	61°38′53″
TMC-1	4 38 20.3	25 42 00
Orion S	5 32 45.4	−05 26 05
Orion-KL	5 32 46.7	−05 24 23
Orion (3N, 1E)	5 33 02.0	−05 21 20
L134N	15 51 30.0	−02 43 31
ρ Oph	16 23 55.0	−24 15 49
Sgr B2 N	17 44 09.5	−28 21 20
Sgr B2(OH)	17 44 11.0	−28 22 30
W49	19 07 51.3	09 01 20
W51 N	19 21 22.2	14 25 17
W51 M	19 21 26.3	14 24 37
B335	19 34 54.0	07 27 20
DR 21 (OH)	20 37 13.8	42 11 53
NGC 7538	23 11 36.7	61 10 47
NGC 7538 IRS 1	23 11 36.0	61 11 47
NGC 7538 IRS 11	23 11 36.1	61 10 30

TABLE 2

N_2H^+ $J = 1 \rightarrow 0$ TRANSITION FREQUENCIES

$F_1'F' \rightarrow F_1F$		ν(MHz)	Relative Intensity
10	11	93171.619	1
12	12	93171.947	5
11	10	93172.078	3
22	11	93173.505	5
23	12	93173.809	7
21	11	93174.016	3
01	12	93176.310	3

[4] The National Radio Astronomy Observatory (NRAO) is operated by Associated Universities, Inc., under contract with the National Science Foundation.

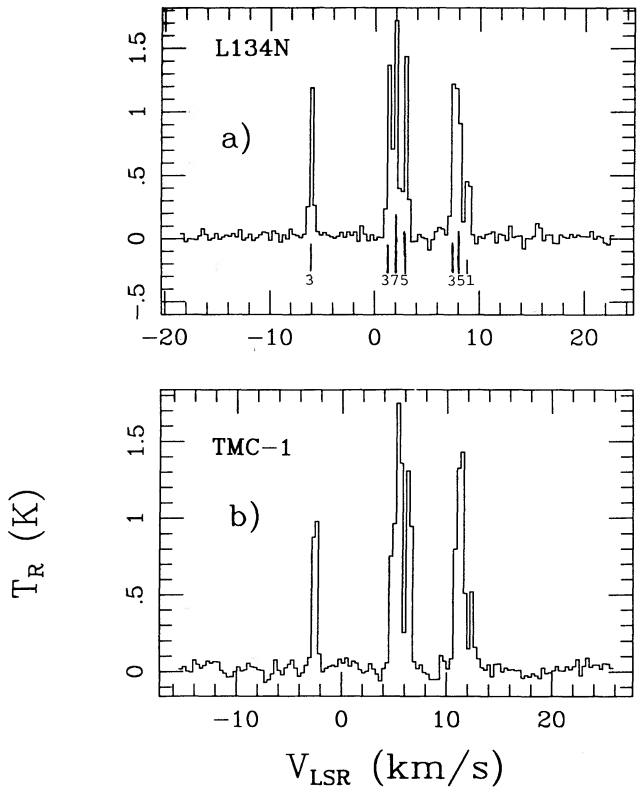

FIG. 1.—Spectrum of the $J = 1 \rightarrow 0$ transition of N_2H^+ observed toward (*a*) L134 N and (*b*) TMC-1, obtained with the NRAO 12 m telescope. Relative strengths of the hyperfine lines are indicated beneath the spectrum of L134 N. Spectral resolution is 100 kHz (0.32 km s^{-1}).

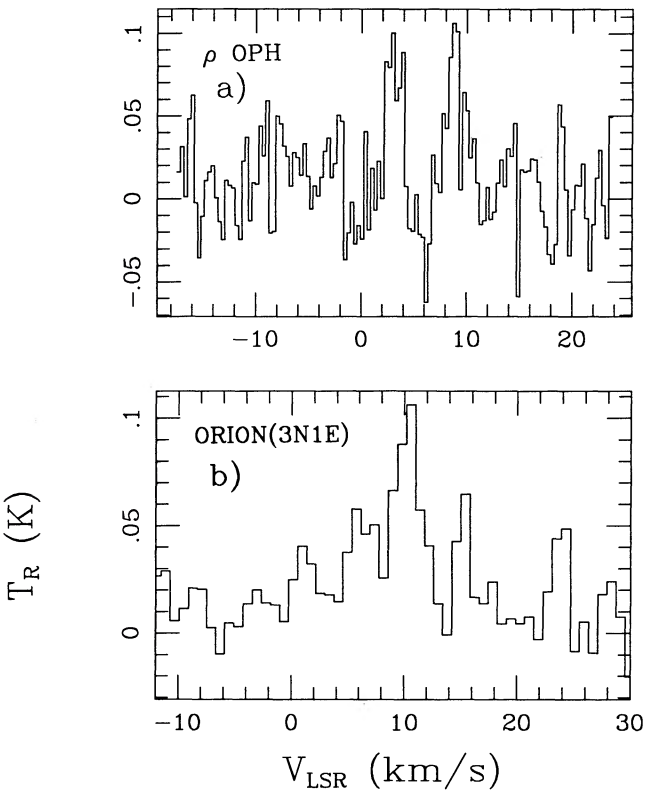

FIG. 2.—Spectrum of the $J = 1 \rightarrow 0$ transition of N_2H^+ observed toward (*a*) ρ Oph and (*b*) Orion (3N, 1E). Spectral resolution is 100 kHz.

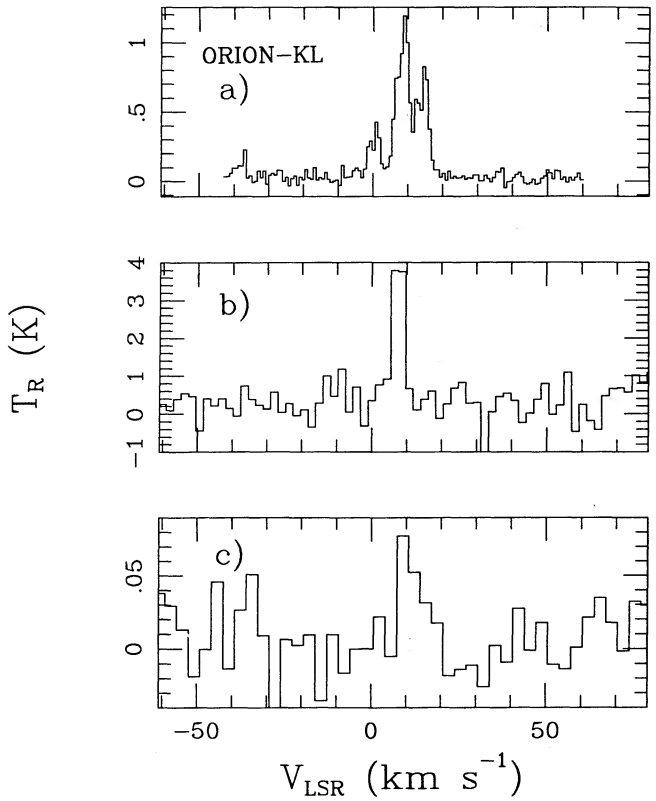

FIG. 3.—Spectra toward Orion-KL of the N_2H^+ (*a*) $J = 1 \rightarrow 0$, (*b*) $J = 3 \rightarrow 2$, and (*c*) the $^{15}NNH^+$ $J = 1 \rightarrow 0$ transitions, with 250 kHz (0.8 km s^{-1}), 2 MHz (2.15 km s^{-1}), and 1 MHz (3.2 km s^{-1}) resolution, respectively. The $J = 1 \rightarrow 0$ spectrum shows evidence of two separate velocity components indicative of two clouds (see Womack et al. 1991; Ziurys et al. 1992).

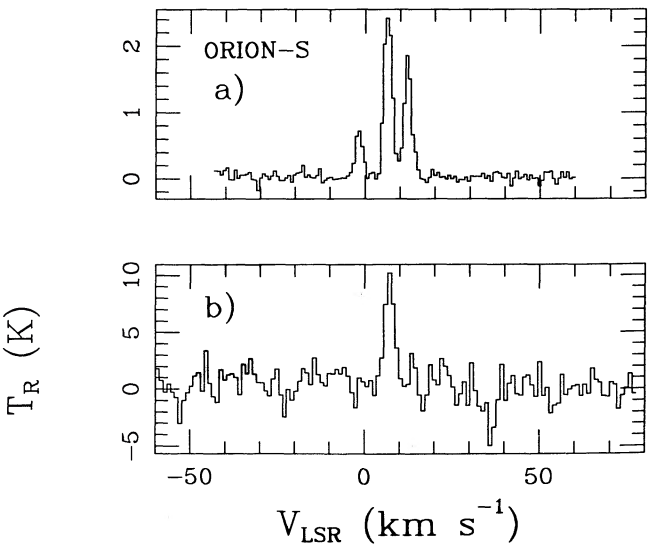

FIG. 4.—Spectra toward Orion-S of the N_2H^+ (*a*) $J = 1 \rightarrow 0$ and (*b*) $J = 3 \rightarrow 2$ transitions. Spectral resolution is 250 kHz (0.8 km s^{-1}) for (*a*) and 1 MHz (1.1 km s^{-1}) for (*b*). Only one velocity component is present in these spectra, taken ~1'.5 south of KL/IRc 2.

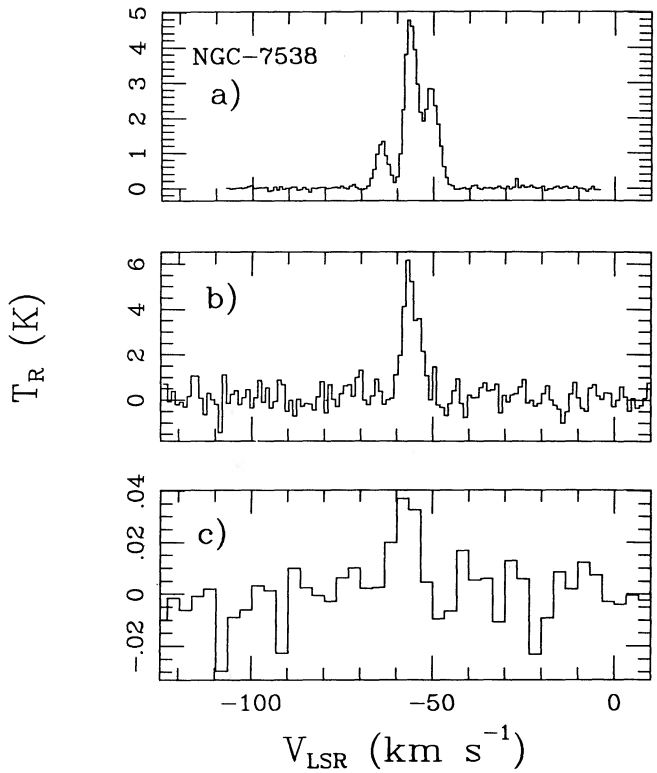

FIG. 5.—Spectrum toward NGC 7538 of the N_2H^+ (*a*) $J = 1 \rightarrow 0$, (*b*) $J = 3 \rightarrow 2$, and (*c*) $N^{15}NH^+$ $J = 1 \rightarrow 0$ transitions. Spectral resolution is 250 kHz for (*a*), and 1 MHz for (*b*) and (*c*). The nitrogen-15 isotope line is clearly present in this source.

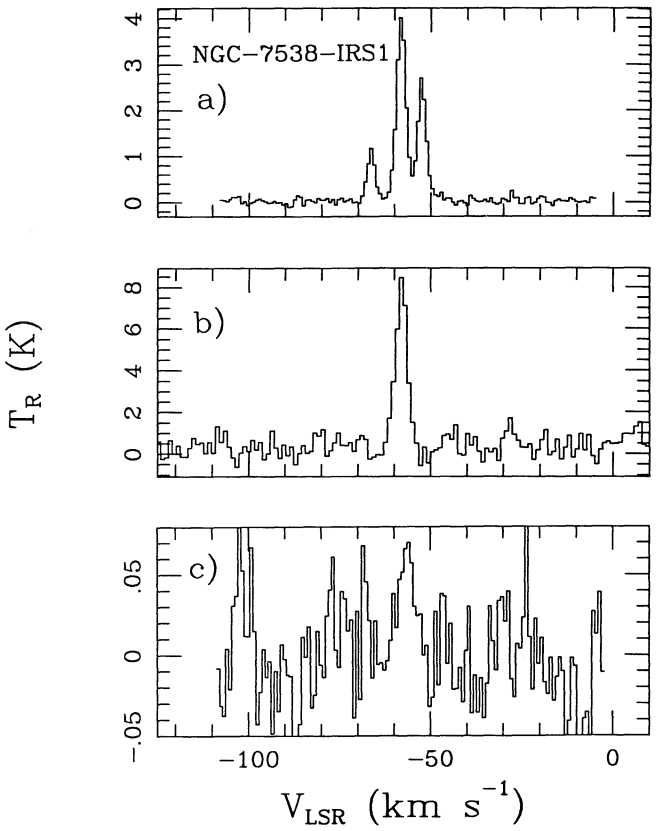

FIG. 6.—Spectrum toward NGC 7538 IRS 1 of the N_2H^+ (*a*) $J = 1 \rightarrow 0$, (*b*) $J = 3 \rightarrow 2$, and (*c*) $^{15}NNH^+$ $J = 1 \rightarrow 0$ transition. Spectral resolution is 250 kHz for (*a*) and (*c*), and 1 MHz for (*b*). No evidence of line wings are present in the spectra, in contrast with CS and HCO^+.

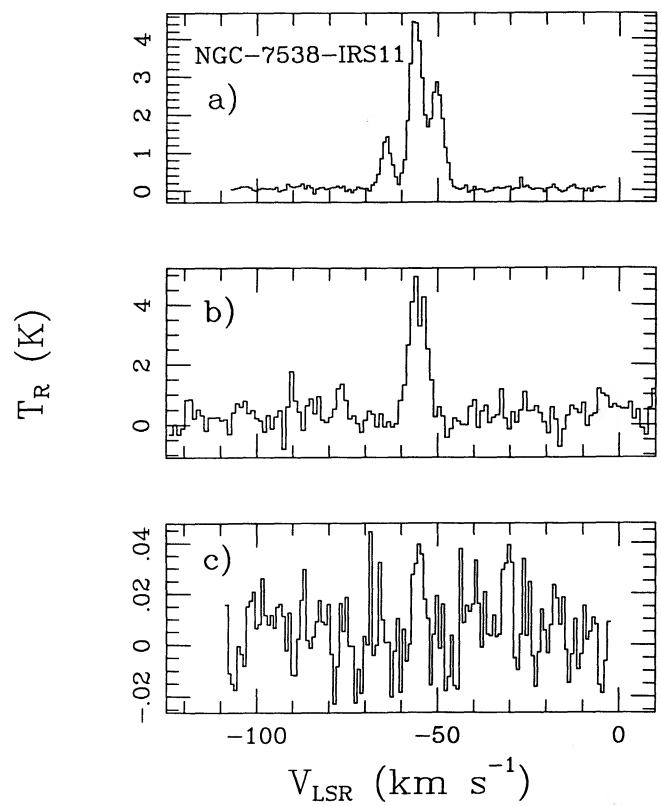

FIG. 7.—Spectrum toward NGC 7538 IRS 11 of the N_2H^+ (*a*) $J = 1 \rightarrow 0$, (*b*) $J = 3 \rightarrow 2$, and (*c*) $^{15}NNH^+$ $J = 1 \rightarrow 0$ transitions. Spectral resolution is 250 kHz for (*a*) and (*c*), and 1 MHz for (*b*).

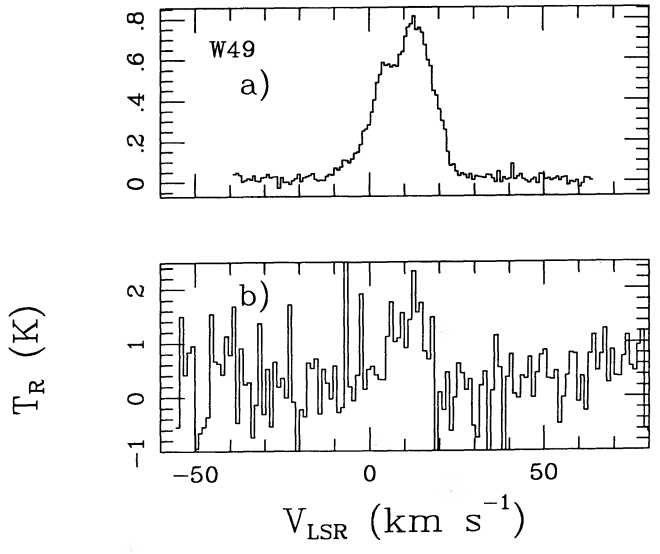

FIG. 8.—Spectra toward W49 of the N_2H^+ (*a*) $J = 1 \rightarrow 0$ and (*b*) $J = 3 \rightarrow 2$ transitions. Spectral resolution is 250 kHz for (*a*) and 1 MHz for (*b*). The $J = 1 \rightarrow 0$ line profile peaks at $V_{LSR} \sim 5$ and 13 km s^{-1}, while the $J = 3 \rightarrow 2$ line appears to have a single peak at ~ 11 km s^{-1}.

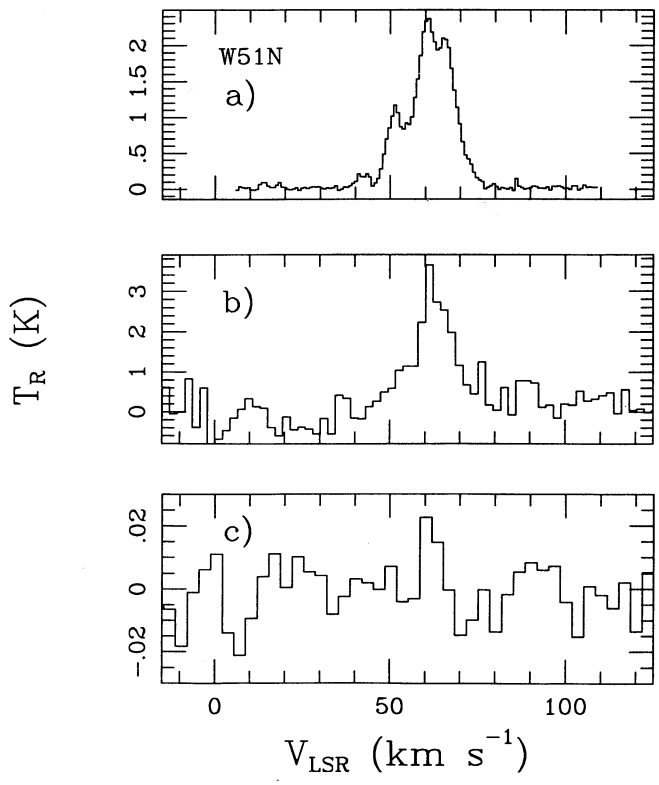

FIG. 9.—Spectrum toward W51 N of the N_2H^+ (*a*) $J = 1 \rightarrow 0$, (*b*) $J = 3 \rightarrow 2$, and (*c*) $^{15}NNH^+$ $J = 1 \rightarrow 0$ transitions. Spectral resolution is 250 kHz for (*a*), 2 MHz for (*b*), and 1 MHz for (*c*). There appears to be a single velocity component in all three transitions at $V_{LSR} \sim 62$ km s^{-1}.

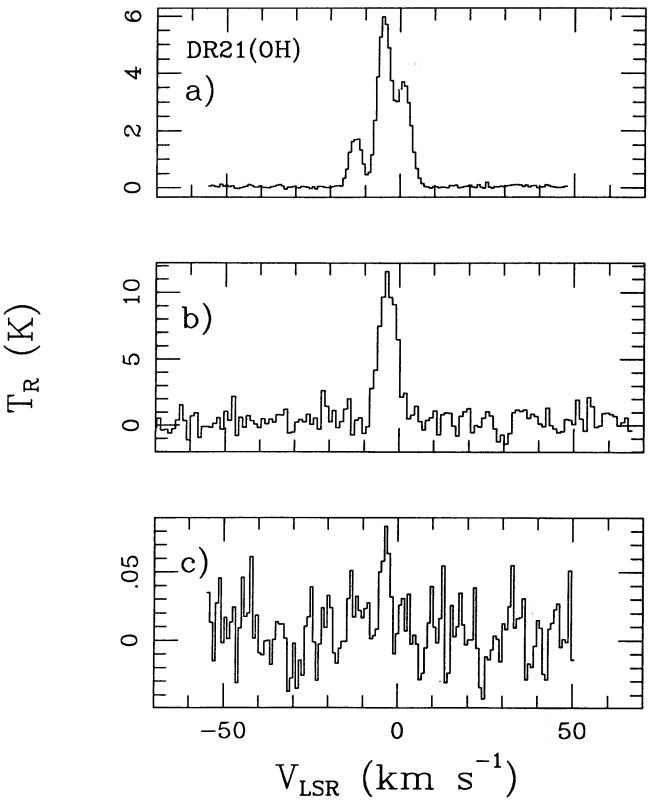

FIG. 11.—Spectrum toward DR 21(OH) of the N_2H^+ (*a*) $J = 1 \rightarrow 0$, (*b*) $J = 3 \rightarrow 2$, and (*c*) $N^{15}NH^+$ $J = 1 \rightarrow 0$ transitions. Spectral resolution is 250 kHz for (*a*) and (*c*), and 1 MHz for (*b*).

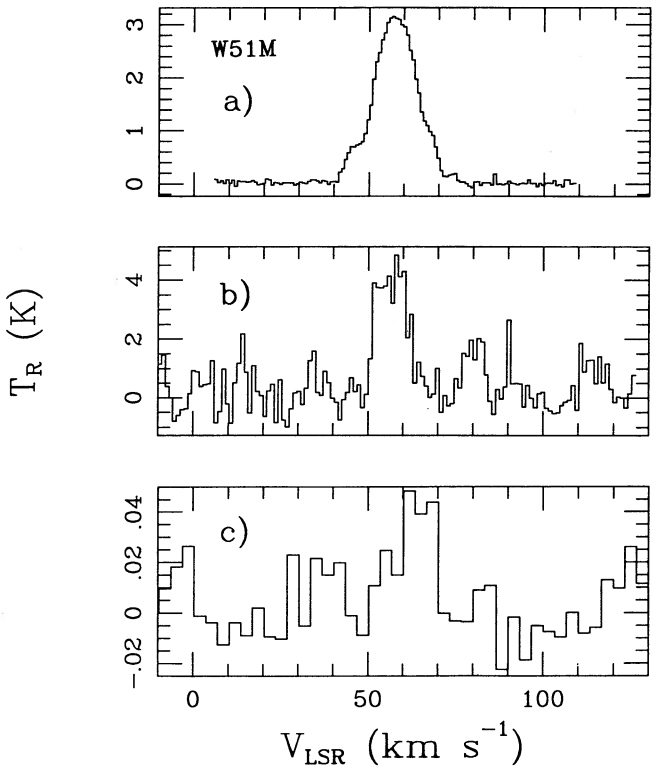

FIG. 10.—Spectrum toward W51 M of the N_2H^+ (*a*) $J = 1 \rightarrow 0$, (*b*) $J = 3 \rightarrow 2$, and (*c*) $^{15}NNH^+$ $J = 1 \rightarrow 0$ transitions. Spectral resolution is 250 kHz for (*a*), and 1 MHz for (*b*) and (*c*). The N_2H^+ $J = 1 \rightarrow 0$ and $J = 3 \rightarrow 2$ transitions both peak at $V_{LSR} \sim 57$ km s^{-1}, while the $^{15}NNH^+$ line has a component at ~ 66 km s^{-1}.

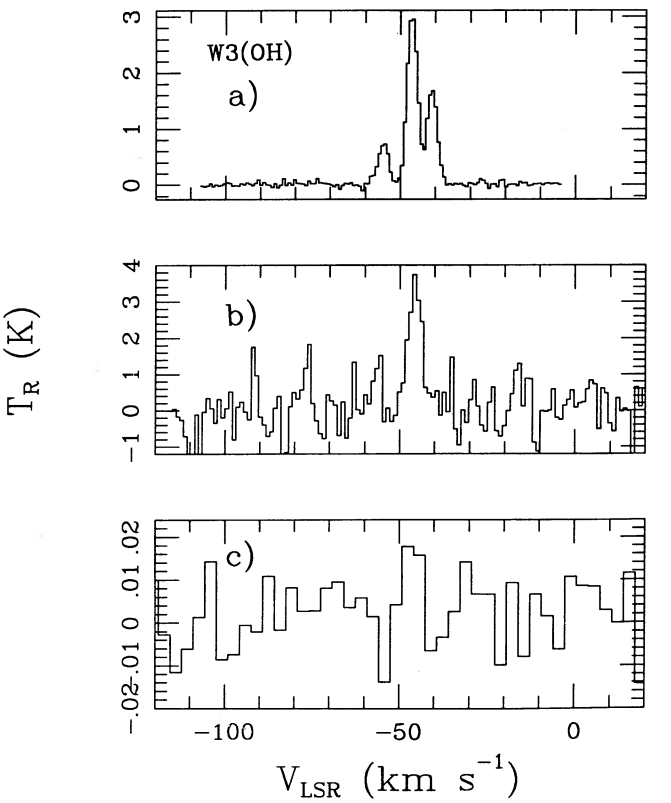

FIG. 12.—Spectrum toward W3(OH) of the N_2H^+ (*a*) $J = 1 \rightarrow 0$, (*b*) $J = 3 \rightarrow 2$, and (*c*) $^{15}NNH^+$ $J = 1 \rightarrow 0$ transitions. Spectral resolution is 250 kHz for (*a*), and 1 MHz for (*b*) and (*c*).

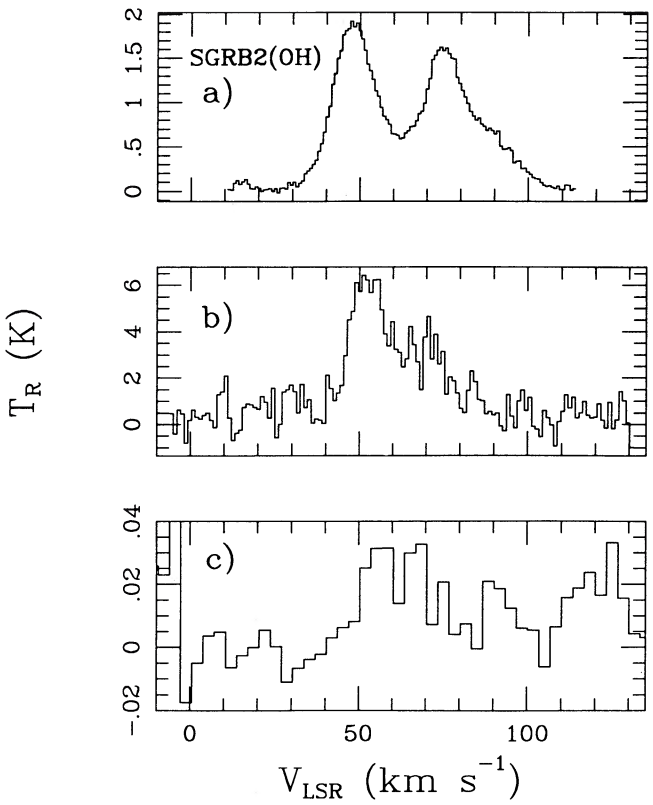

FIG. 13.—Spectra toward Sgr B2(OH) of the N_2H^+ (*a*) $J = 1 \rightarrow 0$, (*b*) $J = 3 \rightarrow 2$, and (*c*) $^{15}NNH^+$ $J = 1 \rightarrow 0$ transitions. Spectral resolution is 250 kHz for (*a*) and 1 MHz for (*b*) and (*c*). Two velocity components were detected in the $J = 1 \rightarrow 0$ line profile, at ~ 75 and 48 km s^{-1}. Two different components are seen in the $J = 3 \rightarrow 2$ transition, at ~ 69 and 52 km s^{-1}. The isotope appears to peak at ~ 69 and 58 km s^{-1}. These differences are likely due to varying beam sizes and/or optical depth effects.

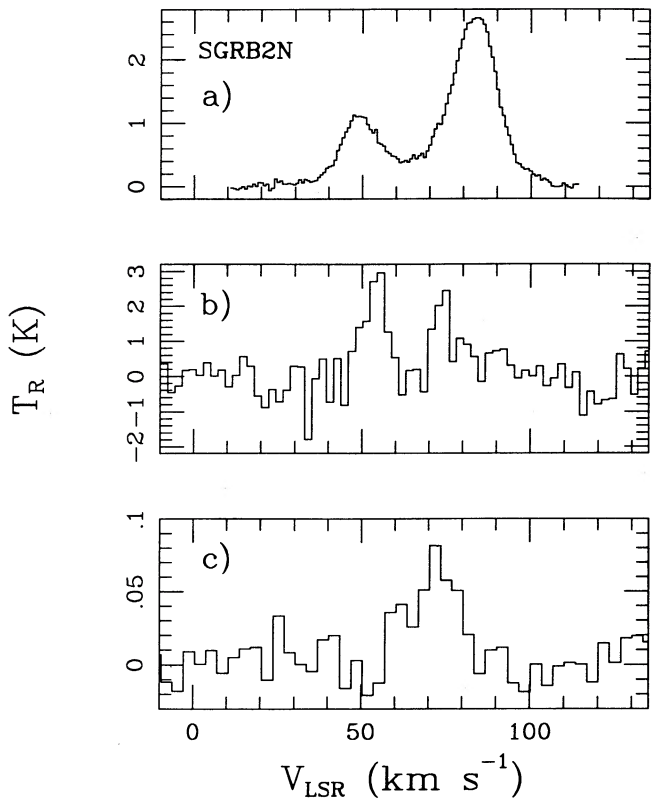

FIG. 14.—Spectrum toward Sgr B2 N of the N_2H^+ (*a*) $J = 1 \rightarrow 0$, (*b*) $J = 3 \rightarrow 2$, and (*c*) $^{15}NNH^+$ $J = 1 \rightarrow 0$ transitions. Spectral resolution is 250 kHz for (*a*), 2 MHz for (*b*), and 1 MHz for (*c*). Two velocity components were detected in the $J = 1 \rightarrow 0$ profile, at ~ 84 and 49 km s^{-1}. Two different velocities were detected in the $J = 3 \rightarrow 2$ transition at 74 and 55 km s^{-1}. The isotope appears to have a single velocity at ~ 75 km s^{-1}. These differences are likely due to varying beam sizes and/or optical depth effects.

TABLE 3

OBSERVATIONS OF THE N_2H^+ $J = 1 \rightarrow 0$ TRANSITION

	T_R (K)								
	$F_1 = 1$–1			$F_1 = 2$–1			$F_1 = 0$–1		
SOURCE	$F = 0$–1	$F = 2$–2	$F = 1$–0	$F = 2$–1	$F = 3$–2	$F = 1$–1	$F = 1$–2	V_{LSR} (km s^{-1})	$\Delta v_{1/2}$ (km s^{-1})
W3(OH)		1.68			2.96		0.72	−46.2	3.15
TMC-1	0.52		1.43	1.30		1.75	0.98	5.5	0.64
Orion-S		1.85			2.42		0.72	6.4	1.91
Orion-KL		0.90			1.14		0.42	9.5	1.0
Orion-KL		0.62			0.77		0.30	7.5	1.7
Orion (3N, 1E)		0.06			0.11		<0.03	10.5	<3.2
L134 N	0.45		1.22	1.43	1.72	1.36	1.19	2.1	0.32
ρ Oph		<0.10			<0.10		<0.05	3.3	2.0
Sgr B2 N				2.65				83.8	15.3
Sgr B2 N				1.11				49.3	14.5
Sgr B2(OH)				1.62				75.2	18.0
Sgr B2(OH)				1.92				48.4	15.1
W49				0.79				13.2	12.6
W49				0.57				5.1	10.6
W51 N		2.10			2.37		1.17	61.1	5.9
W51 M				3.15				57.6	13.5
B335				<0.07				...	...
DR 21 (OH)		3.68			5.98		1.69	−3.8	2.95
NGC 7538		2.83			4.77		1.31	−55.9	3.91
NGC 7538 IRS 1		2.70			4.01		1.16	−57.9	1.70
NGC 7538S IRS 11		2.85			4.47		1.40	−55.8	2.90

TABLE 4

OBSERVATIONS OF THE N_2H^+ $J = 3 \rightarrow 2$ TRANSITION

Source	T_R (K)	V_{LSR} (km s^{-1})	$\Delta v_{1/2}$ (km s^{-1})
W3(OH)	3.74	−45.3	5.2
Orion-S	10.38	6.7	3.2
Orion-KL	4.00	9.0	5.0
L134 N	<1.20	...	...
Sgr B2 N	2.44	74.2	6.7
Sgr B2 N	2.96	55.3	6.4
Sgr B2(OH)	3.42	68.8	11.6
Sgr B2(OH)	5.80	52.3	16.8
W49	1.31	11.1	10.7
W51 N	4.52	61.8	7.5
W51 M	4.45	57.3	10.1
DR 21(OH)	11.59	−2.8	5.2
NGC 7538	6.15	−55.7	5.4
NGC 7538 IRS 1	8.46	−57.5	3.2
NGC 7538 IRS 11	4.94	−55.0	6.5

IRS 1, Orion-KL, Sgr B2 N, Sgr B2(OH), W3(OH), W51 N, and W51 M. The splitting of the hyperfine lines of this transition was less than the resolution of the filterbanks used (Linke et al. 1983) and thus, could not be observed. The $N^{15}NH^+$ $J = 1 \rightarrow 0$ transition (91.205999 GHz) was observed toward DR 21(OH) and NGC 7538. The hyperfine structure of this isotope could have been resolved in the 250 kHz filterbanks. However, the signal was so weak toward both sources that the isotope was clearly apparent only in the 1 MHz filterbanks, which were unable to resolve the hyperfine structure. Thus, toward DR 21(OH) and NGC 7538, a single line was detected, possibly broadened by the blended hyperfine structure. Upper limits to the $^{15}NNH^+$ $J = 1 \rightarrow 0$ emission were obtained for TMC-1, L134 N, Orion (3N, 1E), Orion S, B335, W49, and ρ Oph. Line parameters of the nitrogen-15 isotopes are presented in Table 5.

4. DISCUSSION

4.1. *Column Densities*

Toward some of the dense clouds the N_2H^+ emission may be saturated, and thus, column densities may be underestimated if the opacity is not taken into account. The optical depth can be estimated from analysis of the relative intensities of the hyperfine components of N_2H^+, as well as from the ^{15}N isotope lines (see Swade 1989a). Both methods were used in our analysis.

TABLE 5

OBSERVATIONS OF THE $^{15}NNH^+$ AND $N^{15}NNH^+$ LINES[a]

Source	T_R (K)	V_{LSR} (km s^{-1})	$\Delta v_{1/2}$ (km s^{-1})
W3(OH)	0.02	−44.7	6.3
TMC-1	<0.03	...	...
Orion-S	<0.03	...	...
Orion-KL	0.06	9.0	6.6
Orion (3N, 1E)	<0.04	...	...
L134 N	<0.02	...	...
ρ Oph	<0.03	...	...
Sgr B2 N	0.09	75.4	13.5
Sgr B2(OH)	0.03	68.7	6.7
Sgr B2(OH)	0.03	57.5	10.3
W49	<0.01	...	...
W51 N	0.04	63.7	4.0
W51 M	0.05	66.4	9.8
B335	<0.02	...	...
DR21(OH)[a]	0.08	−3.3	4.1
NGC 7538[a]	0.04	−55.7	6.7
NGC 7538 IRS 1	0.07	−56.3	4.2
NGC 7538 IRS 11	0.04	−55.0	3.8

[a] Denotes measurement of $N^{15}NH^+$ $J = 1 \rightarrow 0$ transition. All others are of the $^{15}NNH^+$ $J = 1 \rightarrow 0$ transition.

Opacities were derived from analysis of the $J = 1 \rightarrow 0$ transitions of N_2H^+ and $^{15}NNH^+$ assuming $^{14}N/^{15}N \sim 300$, found in the outer Galaxy (Wannier, Linke, & Penzias 1981). Where the hyperfine structure of the N_2H^+ $J = 1 \rightarrow 0$ transition could be resolved, the relative intensities of the lines were used to calculate the optical depth as well. In particular, the opacity of the $\Delta F_1 = +1$ component was computed since it was not blended with other nearby hyperfine lines toward most of the sources. Once the optical depth was determined for the $\Delta F_1 = +1$ line, the value was then divided by its statistical weight of $\frac{1}{9}$ in order to calculate the total opacity of the N_2H^+ $J = 1 \rightarrow 0$ transition.

Excitation temperatures for the $J = 1 \rightarrow 0$ transition were measured for the sources for which an N_2H^+ opacity was reasonably estimated. Since no anomalous excitation was observed in the $J = 1 \rightarrow 0$ hyperfine structure, LTE was assumed. The line radiation temperature and optical depth of a single hyperfine line were used to calculate T_{ex} for this transition assuming a unity filling factor. The energy difference between the $J = 1 \rightarrow 0$ hyperfine lines is so small ($< 10^{-8}$ eV) that all hyperfine transitions were assumed to have the same excitation temperature. The calculated values of T_{ex} are given in Table 6.

For sources where both the $J = 3 \rightarrow 2$ and $J = 1 \rightarrow 0$ transitions of N_2H^+ were detected, a column density was calculated using the ratio of the observed radiation temperatures of the two transitions with a large velocity gradient (LVG) analysis. Source sizes were estimated from mapping data of molecules with high dipole moments thought to be excited under similar physical conditions as N_2H^+, such as CS, HCN, and HCO^+. The sources were found to be extended with respect to the telescope beams for all transitions of N_2H^+. Collisional cross sections for N_2H^+ were taken from Green (1975). Typical cloud characteristics for the LVG modeling, such as T_K and $n(H_2)$, were estimated from the literature and are listed in Table 6.

In addition, column densities were calculated analytically. Using the N_2H^+ $J = 1 \rightarrow 0$ transition, the following equation was used to calculate the total column density of the molecule assuming the Rayleigh-Jeans approximation and $\tau \ll 1$:

$$N_{tot} = \frac{3k10^5 T_R \Delta v^{1/2} \zeta_{rot}}{8\pi^3 \mu_0^2 \nu(J+1) e^{-\Delta E_J/T_{rot}}}, \quad (3)$$

where T_{rot} = rotational temperature, ζ_{rot} = rotational partition function, J = lower rotational level, μ_0 = dipole moment of N_2H^+ (3.4 D, Havenith et al. 1990), ν = rest frequency of line, and ΔE_J = energy above ground state. For the cold clouds, a correction due to the cosmic background temperature (T_{bg}) was necessary and the above equation was modified to include $(1 - T_{bg}/T_{ex})$ in the denominator. Rotational temperatures for the warm clouds were estimated from the LVG analysis of the data. For the cold clouds, the rotational temperatures were assumed to be equal to the excitation temperatures (see Table 6). All rotational temperatures used are given in Table 6. For optically thick emission at 3 mm, T_R was substituted by τT_{ex} in equation (3) to calculate a column density.

At 1 mm, the Rayleigh-Jean's approximation was not used and equation (3) was changed to include $e^{h\nu/kT_{ex}}$ in the numerator to calculate column densities. For all sources the emission

TABLE 6

N_2H^+ COLUMN DENSITIES AND FRACTIONAL ABUNDANCES

Source	T_{ex} (K)	T_{rot}[a] (K)	$n(H_2)$[a] (cm^{-3})	T_K[a] (K)	$N(H_2)$ (cm^{-2})	$N(N_2H^+)$ (cm^{-2})	$f(N_2H^+)$
W3(OH)	12.0	12.0	3×10^5	70	2×10^{23}[b]	$(1.5 \pm 1.0) \times 10^{13}$	7×10^{-11}
TMC-1	5.5	5.5	...	...	1×10^{22}[c]	$(7.0 \pm 3.0) \times 10^{12}$	7×10^{-10}
Orion-S	10.7	19.0	8×10^5	100	1×10^{23}[d]	$(2.5 \pm 1.0) \times 10^{13}$	3×10^{-10}
Orion-KL[e]	...	25.0	8×10^5	100	7×10^{23}[f]	$(1.3 \pm 1.0) \times 10^{14}$	2×10^{-10}
Orion (3N, 1E)	...	10.0	...	...	1×10^{22}[c]	$(6.0 \pm 3.0) \times 10^{12}$	6×10^{-10}
L134 N	5.0	5.0	...	...	8×10^{21}[g]	$(5.0 \pm 3.0) \times 10^{12}$	7×10^{-10}
ρ Oph	...	10.0	...	...	2×10^{23}[h]	$(7.0 \pm 3.0) \times 10^{11}$	4×10^{-12}
Sgr B2 N[e]	...	25.0	...	...	1×10^{24}[i]	$(4.0 \pm 3.0) \times 10^{13}$	4×10^{-11}
Sgr B2(OH)[e]	...	25.0	...	...	1×10^{24}[i]	$(3.0 \pm 2.0) \times 10^{13}$	3×10^{-11}
W49	...	15.0	8×10^5	80	1×10^{24}[j]	$(1.5 \pm 0.5) \times 10^{13}$	2×10^{-11}
W51 M	...	30.0	...	...	1×10^{24}[j]	$(1.0 \pm 0.5) \times 10^{15}$	1×10^{-9}
W51 N	5.8	12.0	1×10^5	60	1×10^{24}[j]	$(2.0 \pm 1.5) \times 10^{14}$	2×10^{-10}
B335	...	10.0	...	...	1×10^{21}[k]	$< 1.0 \times 10^{11}$	$< 1 \times 10^{-10}$
DR 21(OH)	14.0	13.0	5×10^5	50	1×10^{23}[l]	$(5.0 \pm 1.5) \times 10^{13}$	5×10^{-10}
NGC 7538	26.0	12.0	2×10^5	200	9×10^{22}[m]	$(2.0 \pm 1.5) \times 10^{13}$	2×10^{-10}
NGC 7538 IRS 1	10.6	15.0	3×10^5	200	9×10^{22}[m]	$(3.0 \pm 2.0) \times 10^{13}$	3×10^{-10}
NGC 7538 IRS 11	27.0	12.0	1×10^5	200	9×10^{22}[m]	$(3.0 \pm 2.0) \times 10^{13}$	3×10^{-10}

[a] Assumed quantity, see text for explanation.
[b] Guilloteau et al. 1983.
[c] Irvine et al. 1985.
[d] Ziurys et al. 1990.
[e] Average of multiple velocity components.
[f] Plambeck et al. 1982.
[g] Swade 1989a.
[h] Loren and Wootten 1986.
[i] Goldsmith, Snell, & Lis 1987; Lis & Goldsmith 1990.
[j] Jaffee, Becklin, & Hildebrand 1984; Jaffee, Harris, & Genzel 1987.
[k] Frerking et al. 1987.
[l] Richardson et al. 1986.
[m] Wilson et al. 1983.

was assumed to be optically thin in the $J = 3 \rightarrow 2$ transition as indicated by an LVG analysis. If the $J = 3 \rightarrow 2$ transition is thick toward a source, then the column density calculated analytically would be underestimated.

4.2. *The Dark Clouds*

L134 N (L183) and TMC-1 are cold dense clouds thought to have T_K and $n(H_2) \sim 10^4$ cm^{-3} (Irvine, Schloerb, & Hjalmarson 1985). L134 N is rich in a wide variety of oxygen-containing species, such as SO_2 and HCO_2H. TMC-1 is a small condensation known to be rich in long carbon chain molecules.

As is seen in Figure 1*a*, the line profiles of the $J = 1 \rightarrow 0$ transition of N_2H^+ toward L134 N and TMC-1 are very narrow. The measured linewidth toward L134 N, $\Delta v_{1/2} = 0.32$ km s^{-1}, and radial velocity, $V_{LSR} = 2.1 \pm$ km s^{-1}, are similar to measurements of other nitrogen-bearing molecules in the region such as NO (McGonagle et al. 1990) and NH_3 and HCN (Swade 1989b). In addition, N_2H^+ was observed toward L134 N by Swade (1989b), who measured $\Delta v_{1/2} = 0.47$ km s^{-1} and $V_{LSR} = 1.83$ km s^{-1} within an arcminute of our source position (for a $J = 1 \rightarrow 0$ rest frequency = 93.17358 GHz).

Toward TMC-1, the N_2H^+ emission has an LSR velocity of 4.8 km s^{-1} and linewidth of 0.64 km s^{-1}. These line parameters are typical of observed emission in this region like NH_3 (Gaida, Ungerechts, & Winnewisser 1984).

Analysis of the observed relative intensities of the hyperfine lines indicate that the N_2H^+ $J = 1 \rightarrow 0$ emission is optically thick toward L134 N ($\tau = 8$) and TMC-1 ($\tau = 5$). Thus, the column densities were calculated under this assumption. The rotational temperatures were taken to be $T_{rot} = 5$ K, which is typically found for molecules with high dipole moments in cold, dark clouds (Swade 1989a).

The excitation temperature for N_2H^+ toward L134 N was calculated to be 5.02 ± 0.25 K, in agreement with that of $T_{ex} = 4.74$ K derived by Swade (1989a) of a position less than one arcminute from our source position. Toward L134 N, a column density of $N_{tot} = (5.2 \pm 3.0) \times 10^{12}$ cm^{-2} was calculated from the $J = 1 \rightarrow 0$ transition of N_2H^+. This agrees well with two values derived by Swade (1987) of $N_{tot} = 5.7 \times 10^{12}$ cm^{-2} and $N_{tot} = 3.8 \times 10^{12}$ cm^{-2}. A fractional abundance of $f \sim 7 \times 10^{-10}$ is derived for N_2H^+. Toward TMC-1, the excitation temperature was calculated to be $T_{ex} = 5.50 \pm 0.40$ K. For this source, a column density of $N_{tot} = (6.9 \pm 3.0) \times 10^{12}$ cm^{-2} was calculated, corresponding to $f \sim 7 \times 10^{-10}$.

The ρ Oph complex of molecular clouds contains several strong infrared sources and dense molecular cores and has a slightly higher kinetic temperature of 10–20 K (Wootten & Loren 1987). Excitation temperatures are also typically ~ 5 K higher than found in most dark clouds. Emission profiles typically are narrow ($\sim$1–2 km s^{-1}) with $V_{LSR} \sim 3.5$ km s^{-1} (Loren, Wootten, & Wilking 1990; Loren 1989).

Only the $\Delta F_1 = -1$ and 0 hyperfine components were detected toward ρ Oph as shown in Figure 2*a*. The N_2H^+ emission was found to be quite strong in this region by Loren & Wootten (1986), in contrast with our data. Comparison of our source position with their mapping data suggests that our N_2H^+ spectrum was obtained at the outer edges of the cloud, which explains its weak intensity.

A column density of $N_{tot} = (6.7 \pm 3.0) \times 10^{11}$ cm^{-2} was calculated analytically for N_2H^+ toward ρ Oph assuming that the emission is optically thin. This corresponds to a fractional abundance of $f \sim 5 \times 10^{-12}$.

No N_2H^+ emission was detected toward the B335, a dark globule thought to contain a compact far-infrared source (Keene et al. 1983). However, an upper limit of $T_R < 0.07$ K was achieved for the $J = 1 \rightarrow 0$ transition. If the transition is assumed to be optically thin and $T_{ex} \sim 10$ K, then an upper limit to the N_2H^+ column density is $N_{tot} < 1 \times 10^{11}$ cm^{-2} and $f < 1 \times 10^{-10}$.

4.3. *Orion-KL, Orion-S, and Orion (3N, 1E)*

The Orion molecular cloud OMC-1 is the nearest and best studied site of star formation and contains several regions of energetic activity. The most closely studied region within OMC-1 is Orion-KL, a $\sim 30''$ area containing hot, dense gas with moderate to high-velocity outflows possibly associated with the young stellar object, IRc 2 (Downes et al. 1981; Plambeck et al. 1982). The surrounding quiescent gas extends several arcminutes north and south of Orion-KL and is usually called the *ridge* or *spike* component, in reference to the very narrow line widths ($\Delta v_{1/2} \sim 2$ km s^{-1}) of molecular emission in this region.

Two velocity components were detected in the 100 kHz spectrum of the N_2H^+ $J = 1 \rightarrow 0$ emission at Orion-KL. They are somewhat visible with 250 kHz resolution (Fig. 3) and clearly seen with 100 kHz resolution (Fig. 15). These velocity components were mapped by Womack et al. (1991). Once component was observed at $V_{LSR} \sim 9.5$ km s^{-1} to the northeast of KL and another to the southwest of KL at $V_{LSR} \sim 7.2$ km s^{-1}. Both components have a line width ~ 1.5 km s^{-1} indicating that the N_2H^+ emission arises from quiescent gas. The presence of two separate clouds is the simplest interpretation of these observations. These spectra are discussed in further detail by Womack et al. (1991).

The spatial distribution of N_2H^+ differs from that of HCO^+ in Orion. For example, while HCO^+ is observed in the 8 and 10 km s^{-1} components of the quiescent ridge gas, with narrow line-widths of ~ 2.5 km s^{-1}, the molecular ion is also observed to have broad line wings of up to 30 km s^{-1}, thought to arise from the moderate and high-velocity outflows near IRc 2 (Vogel et al. 1984). On the other hand, N_2H^+ has narrow line widths (~ 1.5 km s^{-1}) toward Orion-KL, and maps of the region in this ion show the complete absence of any line wings or broadened velocity components (Womack et al. 1991; Ziurys et al. 1992). Both N_2H^+ and HCO^+ are thought to be produced largely by ion-molecule reactions, which typically proceed at low temperatures. The contrast between the two species is thus surprising.

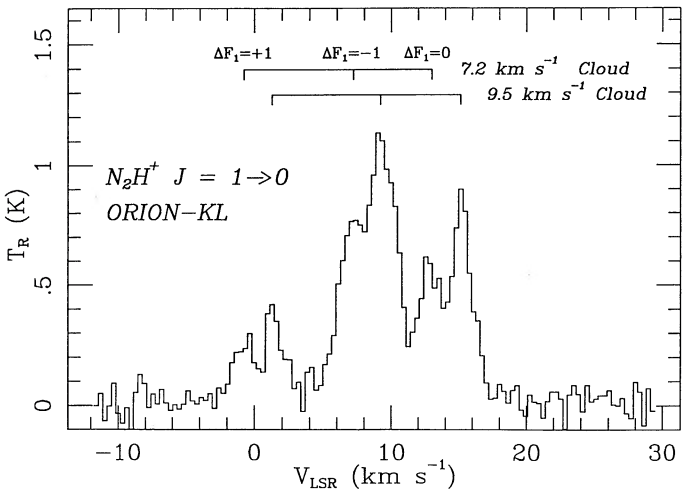

FIG. 15.—Spectrum of the N_2H^+ $J = 1 \rightarrow 0$ transition observed toward Orion-KL. Spectral resolution is 100 kHz (0.32 km s^{-1}). Two velocity components are seen for each of the three ΔF_1 hyperfine lines; one has a radial velocity of $V_{LSR} = 9.5$ km s^{-1} and the other has $V_{LSR} = 7.5$ km s^{-1}. This spectrum suggests the presence of two separate clouds in Orion-KL.

Spectra were also obtained of the N_2H^+ $J = 3 \rightarrow 2$ and $^{15}NNH^+$ $J = 1 \rightarrow 0$ transitions toward Orion-KL, but with lower spectral resolution, as is shown in Figure 3. Thus, a single line was observed for each transition. For the $3 \rightarrow 2$ transition, a line width of 4 km s^{-1} and $V_{LSR} = 9$ km s^{-1} were measured. For the isotope, $V_{LSR} \sim 9.0$ km s^{-1} and $\Delta v_{1/2} = 6.6$ km s^{-1}. An N_2H^+ column density was calculated for Orion-KL both analytically and using the LVG model and was found to be $N_{tot} = (1.5 \pm 1.0) \times 10^{14}$ cm^{-2} corresponding to fractional abundance of $f \sim 2 \times 10^{-10}$. This column density is about an order of magnitude larger than the upper limit of $N_{tot} < 10^{13}$ cm^{-2} measured by Turner & Thaddeus (1977).

An additional site of star formation in Orion has been discovered at $\sim 100''$ to the south of KL. This region, known as Orion S, contains an apparent young stellar object with a bipolar outflow (Ziurys et al. 1990) and hot dust (Keene, Hildebrand, & Whitcomb 1982). Most molecular emission from Orion-S arises from a $V_{LSR} = 6.5$ km s^{-1} component with line widths ~ 3–4 km s^{-1} for $C^{34}S$, CH_3CN, and NH_3 and ~ 6–8 km s^{-1} for SiO (Batrla 1983; Ziurys et al. 1990).

The N_2H^+ emission toward Orion S was found to have a relatively narrow line width of $\Delta v_{1/2} \sim 2.5$ km s^{-1}, with a radial velocity of $V_{LSR} \sim 6.5$ km s^{-1} (see Fig. 4). There is no evidence of line wings, as found in SiO (Ziurys et al. 1990). A column density of $N_{tot} = (2.5 \pm 1.0) \times 10^{13}$ cm^{-2} was calculated using an LVG analysis and a fractional abundance of $f \sim 3 \times 10^{-10}$ is derived for N_2H^+.

Toward the north of Orion-KL is another source considered to be cold and dense called Orion (3N, 1E). The N_2H^+ $J = 1 \rightarrow 0$ line was found to be relatively narrow (~ 3 km s^{-1}) toward this region with $V_{LSR} = 10.5$ km s^{-1} (see Fig. 2*b*). This line profile is similar to those observed for other molecules in the region, such as NH_3, CCH, and CN (Ziurys et al. 1982; Ziurys et al. 1981; Turner & Gammon 1975). These molecules have narrow line widths, but are found at slightly lower velocities of $V_{LSR} = 9.5$–9.9 km s^{-1}. Analysis of the $J = 1 \rightarrow 0$ transition of N_2H^+ and upper limit to $^{15}NNH^+$ indicate that the emission toward Orion (3N, 1E) is optically thin. The N_2H^+ column density was calculated analytically and found to be $N_{tot} = (6.0 \pm 3.0) \times 10^{12}$ cm^{-2}, corresponding to $f = 6 \times 10^{-10}$.

4.4. *NGC 7538, NGC 7538 IRS 1, and NGC 7538 IRS 11*

NGC 7538 is a star-formation region characterized by several compact infrared sources, a bipolar outflow and formaldehyde masers (Pratap, Batrla, & Snyder 1990). Toward the nominal position, the $J = 1 \rightarrow 0$ and $J = 3 \rightarrow 2$ transitions of N_2H^+ were observed to have $\Delta v_{1/2} = 3.9$ km s^{-1} and $V_{LSR} = -55.9$ km s^{-1}, as is seen in Figure 5. This line profile is similar to those observed for other molecules in the region such as HCN and CS (Pratap, Batrla, & Snyder 1989; Kameya et al. 1986). The $^{15}NNH^+$ isotope line was marginally detected, with a line temperature of $T_R = 0.04$ K, indicating that the emission is probably optically thin ($\tau \sim 0.3$). An excitation temperature

of $T_{ex} = 27$ K for the $J = 1 \rightarrow 0$ transition was derived. The N_2H^+ column density was calculated to be $N_{tot} = (2.0 \pm 1.5) \times 10^{13}$ cm^{-2}, corresponding to a fractional abundance of $f \sim 2 \times 10^{-10}$.

As Figure 6 shows, toward NGC 7538 IRS 1 the N_2H^+ emission exhibits a narrow line width of $\Delta v_{1/2} = 1.7$ km s^{-1} with $V_{LSR} = -57.9$ km s^{-1}. The profile of N_2H^+ is about half as broad as that observed toward the nominal position only 1′ to the south. Analysis of the hyperfine line intensity ratios indicates a line opacity of $\tau \sim 1$ and cloud excitation temperature of $T_{ex} \sim 11$ K. A column density of $N_{tot} = (3.0 \pm 2.0) \times 10^{13}$ cm^{-2} was calculated toward this position corresponding to a fractional abundance of $f \sim 3 \times 10^{-10}$.

Toward NGC 7538 IRS 11 all three transitions of N_2H^+ were observed, with a line width of $\Delta v_{1/2} = 2.9$ km s^{-1} and $V_{LSR} = -55.8$ km s^{-1} (see Fig. 7). This profile is slightly broader than the emission at NGC 7538 IRS 1, but less than that of the nominal position. Toward NGC 7538 IRS 1, HCO^+ line profiles have line widths of ~ 2 km s^{-1} with 10 km s^{-1} wings, suggestive of high-velocity outflows (Pratap et al. 1990). Interestingly, none of the N_2H^+ data shows such a line wings. Analysis of the N_2H^+ and $^{15}NNH^+$ $J = 1 \rightarrow 0$ lines and the main isotope's hyperfine lines indicate that the N_2H^+ emission is nearly optically thin ($\tau = 0.25$) and the excitation temperature is $T_{ex} \sim 27$ K. A column density of $N_{tot} = (3.0 \pm 2.0) \times 10^{13}$ cm^{-2} and a fractional abundance of $f \sim 3 \times 10^{-10}$ was found for N_2H^+ toward NGC 7538 IRS 11.

4.5. *W49, W51 N, and W51 M*

W49, W51 N, and W51 M are all regions of active high-mass star formation, characterized by high temperatures and densities. The cloud morphology toward W49 region is difficult to ascertain due to unusual molecular line profiles, which have several disputed explanations. Observations of CO and HCO^+ suggest that two clouds are present along the line of sight—one with a $V_{LSR} = +4$ km s^{-1} and another $+12$ km s^{-1} (Mufson & Liszt 1977; Miyawaki, Hayashi, & Hasegawa 1986; Nyman 1983). However, line profiles of ^{13}CO, $C^{18}O$, and $H^{13}CO^+$ are consistent with emission from a single cloud with $V_{LSR} \sim 7$ km s^{-1} and line widths of ~ 15 km s^{-1} (Mufson & Liszt 1977; Nyman 1984). A dip in emission is observed in the profiles of HCO^+, ^{13}CO, C_2H, CS, and SiO, but not in $H^{13}CO^+$. Thus, it has also been argued that the two apparent velocities in some line profiles are due to self-reversal. In addition, HCO^+ and SiO are both observed to have broad line wings toward W49 (Nyman 1983; Downes et al. 1982).

The N_2H^+ spectra toward W49 also exhibits a complicated profile. As is seen in Figure 8, the $J = 1 \rightarrow 0$ profile peaks at two radial velocities: one with $V_{LSR} \sim +5$ km s^{-1} and another with $V_{LSR} \sim +13$ km s^{-1}. This shape closely resembles that obtained of CS obtained by Miyawaki et al. (1986), which shows the same dip in emission at about ~ 8 km s^{-1}. It is not clear whether the two peaks are due to the presence of two different sources of N_2H^+ emission or whether they are evidence for self-reversal. The $J = 3 \rightarrow 2$ transition of the molecule was marginally detected toward W49 and its profile suggests a single velocity component at $V_{LSR} \sim 10$ km s^{-1} with a line width of ~ 11 km s^{-1}. Although the signal-to-noise ratio is poor, the $J = 3 \rightarrow 2$ profile does appear to arise from the higher velocity component.

The $^{15}NNH^+$ $J = 1 \rightarrow 0$ line was not detected toward W49 down to a limit of $T_R < 0.01$ K. Consequently, the N_2H^+ emission was assumed to be optically thin. A column density was calculated under this assumption to be $N_{tot} = (1.5 \pm 0.5) \times 10^{13}$ cm^{-2} corresponding to a fractional abundance of $f \sim 5 \times 10^{-11}$.

The W51 molecular complex has two regions containing infrared sources associated with H_2O masers: W51 N and W51 M. The $J = 1 \rightarrow 0$ and $J = 3 \rightarrow 2$ transitions of N_2H^+ were detected toward W51 N, and the $J = 1 \rightarrow 0$ line of $^{15}NNH^+$ was marginally detected toward this source, as is seen from Figure 9. The emission for all three transitions was at $V_{LSR} \sim 62$ km s^{-1} with line widths of ~ 4–7 km s^{-1}. The line profiles of N_2H^+ are about half as broad as those observed for other molecules such as CO toward W51 N (e.g., Jaffee, Harris, & Genzel 1987). In addition, there is evidence of emission at ~ 45 km s^{-1} seen in the N_2H^+ $J = 1 \rightarrow 0$ spectrum. Several velocity components have been observed toward W51 in other molecules, including peaks in emission at $V_{LSR} \sim 52$ km s^{-1} in CO and CS, 58 km s^{-1} in CO, CS, and H_2CO and at 66 km s^{-1} in CS, H_2CO, and HCN (e.g., Mufson & Liszt 1979; Penzias et al. 1971; Snyder & Buhl 1971). The N_2H^+ emission toward W51 N peaks at a different velocity, 62 km s^{-1}. An opacity of $\tau = 5$ was determined from the analysis of the individual hyperfine line intensities and also from the isotope data and an excitation temperature of $T_{ex} \sim 6$ K was derived. A column density of N_2H^+ toward this source was found to be $N_{tot} = (2.0 \pm 1.5) \times 10^{14}$ cm^{-2} corresponding to a fractional abundance of $f \sim 7 \times 10^{-10}$.

The W51 M region has been compared with the star-forming environment of Orion-KL (Bally et al. 1987). As Figure 10*a* shows, the N_2H^+ $J = 1 \rightarrow 0$ line profile toward W51 M was found to be unusually shaped with $V_{LSR} \sim 57$ km s^{-1} and $\Delta v_{1/2} = 13.5$ km s^{-1}. This shape cannot be explained by the hyperfine structure. The $J = 3 \rightarrow 2$ transition was also observed at $V_{LSR} \sim 57$ km s^{-1} with a slightly narrower line width of 10.1 km s^{-1} (see Fig. 11*b*). Interestingly, the $^{15}NNH^+$ transition was observed at $V_{LSR} \sim 66$ km s^{-1} with $\Delta v_{1/2} = 9.8$ km s^{-1}, a ~ 9 km s^{-1} shift in velocity from the peak of the main isotope N_2H^+ emission. Thus, there appear to be two components of emission in N_2H^+ toward W51 M. Possible emission at 66 km s^{-1} may explain the shoulder feature on the $J = 1 \rightarrow 0$ line profile in Figure 10*a*. The 66 km s^{-1} velocity component is also seen in H_2CO, CS, and HCN as noted above. Analysis of the main and lesser isotope emission indicates an optical depth of $\tau \sim 5$ for N_2H^+. The column density toward this cloud is $N_{tot} = (1.0 \pm 0.5) \times 10^{15}$ cm^{-2} with $f \sim 5 \times 10^{-10}$.

4.6. *DR 21(OH) and W3(OH)*

DR 21(OH) is a compact molecular cloud associated with H_2O maser activity. All three N_2H^+ transitions were observed toward this source (Fig. 11). The $J = 1 \rightarrow 0$ transition has a line width of ~ 3 km s^{-1} with $V_{LSR} = -3.8$ km s^{-1}, similar to observations made of the molecule in the same region by Linke et al. (1983). Other molecules observed in this region, such as CS and C_2H, have similarly narrow line widths, while HCO^+ and HCN spectra exhibit broad wings (Nyman 1984). N_2H^+ does not exhibit these line wings.

Analysis of the nitrogen-14 and -15 isotope emission and the relative intensities of the N_2H^+ hyperfine lines indicate an optical depth of $\tau \sim 1.5$ toward DR 21(OH), slightly higher than the determination of $\tau = 0.4$ for this source by Linke et al. (1983). An excitation temperature of $T_{ex} \sim 14$ K was calculated for the $J = 1 \rightarrow 0$ transition.

An N_2H^+ column density toward DR 21(OH) was deter-

mined using both the $J = 1 \rightarrow 0$ and $3 \rightarrow 2$ lines in an analytical calculation as well as an LVG analysis and found to be $N_{tot} = (5.0 \pm 1.5) \times 10^{13}$ cm^{-2}. This is in good agreement with the value of $N_{tot} = 6 \times 10^{13}$ cm^{-2}, derived by Linke et al. (1983) from spectra of $^{15}NNH^+$ and $N^{15}NNH^+$ and an assumed $^{14}N/^{15}N$ abundance ratio. A fractional abundance of $f \sim 8 \times 10^{-11}$ is derived for N_2H^+.

W3(OH) is considered to be a site of recent O star formation and includes a very compact H II region. The cloud has a radial velocity of -44.8 km s^{-1} and line widths of ~ 2 km s^{-1} as measured in NH_3 spectra (Reid, Myers, & Bieging 1987). The $J = 1 \rightarrow 0$ and $J = 3 \rightarrow 2$ transitions of N_2H^+ were both found to be relatively strong toward W3(OH) with $V_{LSR} = -47.2$ km s^{-1} and $\Delta v_{1/2} \sim 5$ km s^{-1} (see Fig. 12). The $^{15}NNH^+$ was marginally detected at $V_{LSR} \sim -46$ km s^{-1} with a line width of ~ 6 km s^{-1}. The optical depth was estimated from analysis of the hyperfine line intensities, as well as comparison of the main and isotope lines of the $J = 1 \rightarrow 0$ transition, and found to be thin. A column density of $N_{tot} = (1.3 \pm 1.0) \times 10^{13}$ cm^{-2} was calculated for N_2H^+ toward W3(OH) corresponding to a fractional abundance of $f \sim 7 \times 10^{-11}$.

4.7. *Sgr B2(OH) and Sgr B2 N*

Virtually all interstellar molecules discovered to date have been observed toward the giant molecular clouds associated with the compact H II region Sgr B2. This source, located only ~ 120 pc from the Galactic center, is a site of massive star formation and has a very complicated cloud structure, as is shown in the spectra of many molecules (e.g., Cummins, Linke, & Thaddeus 1986). Likewise, a complex velocity structure was observed in the N_2H^+ emission toward the Sgr B2 clouds.

Toward Sgr B2(OH) what appear to be two velocity components were detected in the $J = 1 \rightarrow 0$ transition of N_2H^+: one with $V_{LSR} = 75$ km s^{-1} and another at $V_{LSR} = 48$ km s^{-1}, both with approximately the same line width of $\Delta v_{1/2} = 15$ km s^{-1} (see Fig. 13). These two components were observed in N_2H^+ by Turner & Thaddeus (1977) and have also been seen in other molecules such as HCN, HCO^+, CH_3OH, and SiO. However, the $J = 3 \rightarrow 2$ transition was detected at ~ 53 km s^{-1} with a hint of emission at ~ 71 km s^{-1}. The discrepancy between the $J = 1 \rightarrow 0$ and $J = 3 \rightarrow 2$ line profiles may be due to the differing beam sizes at the respective frequencies, or possibly optical depth effects. These two velocities were also seen in HC_3N. In the $^{15}NNH^+$ emission, only a broad component was observed near $V_{LSR} \sim 61$ km s^{-1}. This velocity corresponds to the dip in the main isotope spectrum and may indicate self-reversal in the main line.

Toward Sgr B2 N, the N_2H^+ emission also arises from several velocity components. The $J = 1 \rightarrow 0$ profile has two peaks, one at 83 km s^{-1} and another at 50 km s^{-1} as is shown in Figure 14. The higher velocity emission is about 2.5 times as strong as the 50 km s^{-1} component. Two different velocities are apparent in the $J = 3 \rightarrow 2$ emission—one at 55 km s^{-1} and another at 74 km s^{-1}. Both of the velocity components in the $3 \rightarrow 2$ emission are much narrower than those of the $J = 1 \rightarrow 0$ emission. Again, varying beam sizes and optical depth effects are likely to account for the differences in these two spectra. The $^{15}NNH^+$ emission was detected only in the 74 km s^{-1} component apparent in the $J = 3 \rightarrow 2$ line.

Interpretation of the N_2H^+ spectra is difficult due to the many different velocity components in these two clouds. Because of the discrepancies in the $J = 1 \rightarrow 0$ and $J = 3 \rightarrow 2$ line profiles, an LVG analysis was not performed for the Sgr B2 sources. Instead, column densities were calculated from the individual rotational lines using the optically thin approximation and assumed rotational temperatures. Because the $J = 1 \rightarrow 0$ line may be optically thick, the column densities may be underestimated. Average column densities were found to be $N_{tot} = (3.0 \pm 2.0) \times 10^{13}$ cm^{-2} for Sgr B2(OH) and $N_{tot} = (4.0 \pm 3.0) \times 10^{13}$ cm^{-2} for Sgr B2 N corresponding to fractional abundances of 3×10^{-11} and 4×10^{-11}, respectively. Again, these values are likely to be underestimated.

4.8. *Implications for Ion-Molecule Chemistry*

Ion-molecule models predict that molecular ions should be produced primarily in cold, quiescent gas. The only molecular ion in dense gas which has been previously studied in detail is HCO^+, which is abundant in cold, unperturbed regions. For example, spectra of the HCO^+ $J = 1 \rightarrow 0$ transition obtained toward Orion-KL, DR 21(OH), and NGC 7538 have relatively narrow line widths ($\Delta v_{1/2} = 2$–4 km s^{-1}) characteristic of emission from cold, quiescent regions, However, the HCO^+ line profiles also exhibit broad line wings of 10–25 km s^{-1} (Vogel et al. 1984; Nyman 1984; Pratap et al. 1990). Such extended line wings are indicative of emission arising from hot, perturbed gas in outflows. Thus, the chemical behavior of HCO^+ cannot be explained entirely by ion-molecule models.

On the other hand, our survey shows that N_2H^+ is present overwhelmingly in quiescent regions. This is shown by the narrow line-widths observed ($\Delta v_{1/2} \lesssim 3$–$5$ km s^{-1}) for N_2H^+ and the generally low-excitation temperatures ($T_{ex} < 20$ K) of the $J = 1 \rightarrow 0$ transition. Also, there are no line wings observed in any of the N_2H^+ spectra, even toward sources where HCO^+ exhibits them quite prominently. In addition, LVG modeling results of the $J = 1 \rightarrow 0$ and $J = 3 \rightarrow 2$ transitions suggest that N_2H^+ is present in gas of moderate density, $n(H_2) \sim 10^5$ cm^{-3} (see Table 6), consistent with ion-molecule models, which predict molecular ions to be destroyed as densities increase [$n(H_2) > 10^6$ cm^{-3}]. The chemical behavior of N_2H^+ thus appears to be well-explained by ion-molecule models.

The differences between HCO^+ and N_2H^+ are puzzling. This is particularly true since HCO^+ is produced and destroyed in a similar manner to N_2H^+. It is formed by the reaction

$$CO + H_3^+ \rightarrow HCO^+ + H_2 \qquad (4)$$

and destroyed by electron recombination. However, in more diffuse shocked gas, HCO^+ is thought to also be formed by reactions of C^+ (Mitchell & Deveau 1983), i.e., by formation routes not available to N_2H^+. Perhaps this may explain the absence of N_2H^+ in shocked outflow material. Observations probing possible correlations of HCO^+ with C I and C^+ may be helpful in clarifying the chemistry of HCO^+.

The fractional abundances of N_2H^+ in the dense clouds observed have a mean value of $f = (3.6 \pm 3.1) \times 10^{-10}$. Within the errors, there is no appreciable difference between the ion's abundances in dark and warm clouds. This is additional evidence for the production of N_2H^+ in quiescent gas. Curiously, these abundances correspond to those predicted by models of ion-molecule chemistry which have reached steady state. For example, early time models predict fractional abundances for N_2H^+ of $f \sim 10^{-13}$ to 10^{-12}, while the steady state models predict $f \sim 10^{-11}$ to 10^{-10} (Millar 1990; Herbst & Leung 1989; Brown & Rice 1986).

4.9. N_2H^+ and Interstellar Nitrogen Chemistry

It is significant that N_2H^+ abundances in both warm and cold dense clouds are better reproduced by ion-molecule models which have reached steady state. As mentioned, NH_3 abundances in dense clouds are also better predicted by models of steady state rather than of early times (Millar 1990). However, dense cloud abundances of NO appear well explained by models of early time chemistry (Ziurys et al. 1991). The differences between the model predictions of N_2H^+, NH_3, and NO may be due to the different formation pathways. The production of NO in dense clouds is thought to be from the neutral neutral reaction

$$N + OH \rightarrow NO + H \quad (5)$$

(Pineau des Forêts, Roueff, & Flower 1990; Millar 1990). Molecular nitrogen can then be produced via

$$NO + N \rightarrow N_2 + O\,. \quad (6)$$

At this point, N_2H^+ can be formed from N_2 according to equation (1). The direct link between the N_2 and NO production suggests that the abundances of both molecules should be predicted best by the same type of ion-molecule chemical model. Thus, it is difficult to understand why NO abundances are better fit by early time models, while N_2H^+ abundances indicate a steady state model is more appropriate.

Another set of reactions, initiated by carbon-bearing rather than oxygen-bearing molecules, has been suggested for the production of N_2H^+ (Nejad et al. 1990). In this model, the following reaction sequence

$$CH \xrightarrow{N} CN \xrightarrow{N} N_2 \quad (7)$$

and equation (1) is considered to be the most important route to N_2H^+ formation. Once N_2 has been formed, ammonia is considered to be produced primarily from the following reaction

$$N_2 \xrightarrow{He^+} N^+ \xrightarrow{H_2} NH^+ \xrightarrow{H_2} NH_2^+ \xrightarrow{H_2} NH_3^+ \xrightarrow{H_2} NH_4^+ \xrightarrow{e^-} NH_3\,. \quad (8)$$

Thus, perhaps the agreement of N_2H^+ and NH_3 abundances with steady state models is due to a nitrogen chemistry initiated by reactions with carbon-based species, as opposed to the usual assumption of oxygen-based molecules as precursors. In order to better understand the chemistry of simple nitrogen-bearing molecules, more studies of the spatial distribution and line profiles of NO and N_2H^+ are needed. In addition, comparison of CN, CH, and N_2H^+ data may be helpful in examining formation pathways in nitrogen chemistry.

4.10. N_2H^+: A Tracer of Quiescent Gas?

These observations do suggest that N_2H^+ appears to be an excellent tracer of quiescent gas. This is shown by the narrow line widths found in both transitions of the ion, its low-excitation temperatures, and the lack of appreciable difference in abundances in warm and cold clouds. Such behavior is predicted from ion-molecule chemistry, but as discussed, is not found for HCO^+. In fact, molecules normally used to trace large-scale structure of clouds such as CO, CS, HCO^+, and HCN are usually present both in hot and cold material. Thus, they are not very selective as tracers of extended gas, unlike N_2H^+. N_2H^+ sharply contrasts the chemical behavior of SiO, which appears to be present only in hot, disturbed gas (Ziurys, Friberg, & Irvine 1989).

5. CONCLUSIONS

Our survey of N_2H^+ toward both warm and cold clouds suggests that there is little difference in the chemical behavior of this species in the two cloud types. Column densities of N_2H^+ calculated from the data were found to be $N_{tot} \sim 5 \times 10^{12}$ cm^{-2} for the cold clouds and $N_{tot} \sim 1 \times 10^{14}$ cm^{-2} for the warm clouds. However, fractional abundances of N_2H^+ with respect to H_2 were found to be fairly uniform between the two classes of objects, with typically $f \sim 6 \times 10^{-10}$ for cold clouds and $f \sim 3 \times 10^{-10}$ for warm regions, with an average of $f \sim 4 \times 10^{-10}$. Also, N_2H^+ in all sources was found to exhibit narrow line widths and low-excitation temperatures. No evidence for the presence of the ion in hot, shocked outflows was found. Thus the abundance and distribution of N_2H^+ is well-explained by quiescent cloud, ion-molecule chemistry. However, the observed abundances of this species compare better with ion-molecule model calculations which have reached "steady state," versus those at "early times." Interestingly, observed abundances of NH_3 are also better produced by steady state models. Thus, the chemistry of nitrogen and hydrogen containing compounds in quiescent gas may have reached steady state.

M. W. and S. W. acknowledge NSF grant AST-8820145. L. M. Z. acknowledges NSF grant AST 90-58467. M. W. also acknowledges a GSARDP grant from the Office of the Vice President at Arizona State University.

REFERENCES

Amano, T. 1990, J. Chem. Phys., 92, 6492
Bally, J., Langer, W. D., Stark, A. A., & Wilson, R. W. 1987, ApJ, 312, L45
Batrla, W., Wilson, T. L., Bastien, P., & Ruf, K. 1983, A&A, 128, 279
Brown, R. D., & Rice, E. H. N. 1986, MNRAS, 223, 405
Cazzoli, G., Corbelli, G., Degli Esposti, C., & Favero, P. G. 1985, Chem. Phys. Lett., 118, 164
Cummins, S. E., Linke, R. A., & Thaddeus, P. 1986, ApJS, 60, 819
Downes, D., Genzel, R., Becklin, E. E., & Wynn-Williams, C. G. 1981, ApJ, 244, 869
Downes, D., Genzel, R., Hjalmarson, Å., Nyman, L.-Å., & Rönnäng, B. 1982, ApJ, 252, L29
Frerking, M. A., Langer, W. D., & Wilson, R. W. 1987, ApJ, 313, 320
Gaida, M., Ungerechts, H., & Winnewisser, G. 1984, A&A, 137, 17
Goldsmith, P. F., Snell, R. L., & Lis, D. C. 1987, ApJ, 313, L5
Green, S. 1975, ApJ, 201, 366
Green, S., Montgomery, J. A., Jr., & Thaddeus, P. 1974, ApJ, 193, L89
Guilloteau, S., Stier, M. T., & Downes, D. 1983, A&A, 126, 10
Havenith, M., Zwart, E., Meerts, W. L., & ter Meulen, J. J. 1990, J. Chem. Phys., 93, 8446
Herbst, E., & Klemperer, W. 1973, ApJ, 185, 505
Herbst, E., & Leung, C. M. 1989, ApJS, 69, 271
Irvine, W. M., Schloerb, F. P., & Hjalmarson, Å. 1985, in Protostars and Planets II, ed. D. C. Black & M. S. Matthews (Tucson: Univ. of Arizona), 579
Jaffee, D. T., Becklin, E. E., & Hildebrand, R. H. 1984, ApJ, 279, L51
Jaffee, D. T., Harris, A. I., & Genzel, R. 1987, ApJ, 316, 231
Kameya, O., Hasegawa, T. I., Hirano, N., Tosa, M., Taniguchi, Y., & Takakubo, K. 1986, PASJ, 38, 793
Keene, J., Davidson, J., Harper, D. A., Hildebrand, R. H., Jaffee, D. T., Loewenstein, R. F., Low, F. J., & Pernic, R. 1983, ApJ, 274, L43
Keene, J., Hildebrand, R. H., & Whitcomb, S. E. 1982, ApJ, 252, L11
Linke, R. A., Guélin, M., & Langer, W. D. 1983, ApJ, 271, L85

Lis, D. C., & Goldsmith, P. F. 1990, ApJ, 356, 195
Loren, R. B. 1989, ApJ, 338, 902
Loren, R. B., & Wootten, A. 1986, ApJ, 306, 142
Loren, R. B., Wootten, A., & Wilking, B. A. 1990, ApJ, 365, 269
Mauersberger, R., Henkel, C., Wilson, T. L., & Walmsley, C. M. 1986, A&A, 162, 199
McGonagle, D., Ziurys, L. M., Irvine, W. M., & Minh, Y. C. 1990, ApJ, 359, 121
Millar, T. J. 1990, in Molecular Astrophysics, ed. T. W. Hartquist (Cambridge: Cambridge Univ. Press), 115
Millar, T. J., DeFrees, D. J., McLean, A. D., & Herbst, E. 1988, A&A, 194, 250
Mitchell, G. F., & Deveau, T. J. 1983, ApJ, 266, 646
Miyawaki, R., Hayashi, M., & Hasegawa, T. 1986, ApJ, 305, 353
Mufson, S. L., & Liszt, H. S. 1977, ApJ, 212, 664
———. 1979, ApJ, 232, 451
Nejad, L. A. M., Williams, D. A., & Charnley, S. B. 1990, MNRAS, 246, 183
Nyman, L.-Å. 1983, A&A, 120, 307
———. 1984, A&A, 141, 323
Penzias, A. A., Solomon, P. M., Wilson, R. W., & Jefferts, K. B. 1971, 168, L53
Pineau des Forêts, G., Roueff, E., & Flower, D. R. 1990, MNRAS, 244, 668
Plambeck, R. L., Wright, M. C. H., Welch, W. J., Bieging, J. H., Baud, B., Ho, P. T. P., & Vogel, S. N. 1982, ApJ, 259, 617
Pratap, P., Batrla, W., & Snyder, L. E. 1989, ApJ, 341, 832
———. 1990, ApJ, 351, 530
Reid, M. J., Myers, P. C., & Bieging, J. H. 1987, ApJ, 312, 830
Richardson, K. J., White, G. J., Phillips, J. P., & Avery, L. W. 1986, MNRAS, 219, 167
Sastry, K. V. L. N., Helminger, P., Herbst, E., & De Lucia, F. C. 1981, Chem. Phys. Lett., 84, 286
Snyder, L. E., & Buhl, D. 1971, ApJ, 163, L47
Swade, D. A. 1987, Ph.D., thesis, Univ. of Massachusetts
Swade, D. A. 1989a, ApJ, 345, 828
———. 1989b, ApJS, 71, 219
Thaddeus, P., & Turner, B. E. 1975, ApJ, 201, L25
Turner, B. E. 1974, ApJ, 193, L83
Turner, B. D., & Gammon, R. H. 1975, ApJ, 198, 71
Turner, B. E., & Thaddeus, P. 1977, ApJ, 211, 755
Vogel, S. N., Wright, M. C. H., Plambeck, R. L., & Welch, W. J. 1984, ApJ, 283, 655
Wannier, P. G., Linke, R. A., & Penzias, A. A. 1981, ApJ, 247, 522
Wilson, T. L., Mauersberger, R., Walmsley, C. M., & Batrla, W. 1983, A&A, 127, L19
Womack, M., Ziurys, L. M., & Wyckoff, S. 1991, ApJ, 370, L99
Wootten, A., & Loren, R. B. 1987, ApJ, 317, 220
Ziurys, L. M., Friberg, P., & Irvine, W. M. 1989, 343, 201
Ziurys, L. M., Martin, R. N., Pauls, T. A., & Wilson, T. L. 1981, A&A, 104, 288
Ziurys, L. M., McGonagle, D., Minh, Y., & Irvine, W. M. 1991, ApJ, 373, 535
Ziurys, L. M., Saykally, R. J., Plambeck, R. L., & Erickson, N. R. 1982, ApJ, 254, 94
Ziurys, L. M., Wilson, T. L., & Mauersberger, R. 1990, ApJ, 356, L25
Ziurys, L. M., Womack, M., Wyckoff, S., & Sage, L. J. 1992, in preparation